Depression of quantal size of GABAergic synaptic transmission in the insular cortex by the reduction of peripheral unmyelinated C-fibers

Shota Murayama
Nihon University Graduate School of Dentistry
Major in Endodontics
(Directors: Profs. Bunnai Ogiso and Masayuki Kobayashi,
and Assis. Prof. Kiyofumi Yamamoto)

Index

This thesis is based on the following article and additional results in terms of miniature inhibitory postsynaptic currents of fast-spiking neuron (Fig. 3):

Shota Murayama, Kiyofumi Yamamoto, Bunnai Ogiso, Masayuki Kobayashi (2017) Ablation of C-fibers decreases quantal size of GABAergic synaptic transmission in the insular cortex. Neuroscience, 365:179-191.

Abstract

The primary sensory cortex exhibits neuroplastic changes responding to sensory disturbances, and GABAergic synaptic transmission plays a critical role in the regulation of plasticity. The insular cortex (IC) integrates orofacial nociceptive signals conveyed via myelinated Aδ- and unmyelinated C-fibers. However, it has been unknown whether a disturbance of nociceptive inputs, such as a deletion of the peripheral nerves, alters GABAergic local circuit in IC. The present study elucidated GABAergic synaptic transmission in the model rat whose C-fibers were ablated by capsaicin injection 1-2 days after birth. *In vivo* optical imaging revealed that capsaicin-treated rats showed a facilitative excitatory propagation in IC responding to dental pulp stimulation. Whole-cell patch-clamp recording from pyramidal (Pyr) and fast-spiking (FS) neurons demonstrated that capsaicin-treated rats showed the smaller amplitude of miniature inhibitory postsynaptic currents (IPSCs) than sham-treated rats without changing the frequency. Furthermore, replacement of extracellular Ca^{2+} to Sr^{2+}, which induces an asynchronous release of neurotransmitters in the quantal size, induced a smaller amplitude of asynchronous unitary IPSCs recorded from FS to Pyr connections in capsaicin-treated rats than sham-treated rats. These results suggest that capsaicin treatment depresses IPSCs via a postsynaptic mechanism. To confirm this possibility, the variance-mean analysis of unitary IPSCs was employed and I found that quantal size of GABAergic synaptic transmission was smaller in capsaicin-treated rats than in sham-treated rats. These results suggest that reduction of C-fibers induces plastic changes in GABAergic synaptic transmission by decreasing postsynaptic $GABA_A$ receptor-mediated conductance, which is a possible mechanism of the facilitative excitation in IC of capsaicin-treated rats.

Introduction

The insular cortex (IC) receives multimodal sensory inputs including gustation, visceral sensation, nociception, thermal sensation, and audition (Yamamoto, 1984; Yasui et al., 1991; Nakamura et al., 2015), and is considered to integrate these sensory information processing (Gogolla et al., 2014). The insular oral region (IOR) is located dorsal to the rhinal fissure and caudal to the middle cerebral artery, and is activated by electrical stimulation of the dental pulp and periodontal ligament (Remple et al., 2003; Horinuki et al., 2015; Nakamura et al., 2015; Horinuki et al., 2016; Nakamura et al., 2016), which involves nociceptive fibers, Aδ- and C-fibers. Extracellular recordings from IOR neurons demonstrate a wide variation of the latency of action potential induction from the onset of electrical stimulation of the dental pulp, suggesting that noxious information from both Aδ- and C-fibers project to IOR neurons (Nakamura et al., 2015). However, it has been still unknown how the noxious information is temporally and spatially processed in IOR.

Maladaptive processes by various pathophysiological diseases such as neural inflammation, nerve injury and trauma, and growing tumor convert acute pain to chronic pain (Kuner and Flor, 2016). Under these conditions, neuroplastic changes occur not only in the peripheral nervous system but also in the central nervous system, including the cerebral cortex. Zhou and his colleagues have demonstrated that long-term potentiation and other types of synaptic changes are induced in the anterior cingulate cortex and IC of the chronic pain models (Bliss et al., 2016). Therefore, it is essential for elucidating the neural mechanisms of chronic pain to understand plastic changes of the cerebrocortical local circuits in the animals with nociceptive disorders.

Capsaicin, an agonist of transient receptor potential vanilloid 1 (TRPV1), activates TRPV1 receptor channels (Caterina and Julius, 2001), and subcutaneous injection of capsaicin at neonatal period decreases peripheral fibers with small diameter and primary neurons containing calcitonin gene-related peptide (CGRP; Wimalawansa, 1993; Cavanaugh et al., 2009), suggesting that capsaicin treatment may induce a loss of C-fibers (Nagy et al., 1983). Therefore, the capsaicin-treated animals at the neonatal period are considered to be a suitable model for examining the effects of an imbalance of noxious inputs, in this case, a selective loss of C-fibers. The present study aims to

examine the effects of disproportional noxious inputs on the GABAergic synaptic transmission in IC, focusing on inhibitory synapses from fast-spiking interneurons (FS) to pyramidal neurons (Pyr), which play a central role in regulating excitation in the cerebral cortex. I evaluated the precise profiles of FS→Pyr connections in the capsaicin-treated rat (CAP) by paired whole-cell patch-clamp recording of the unitary component of $GABA_A$ receptor-mediated inhibitory synaptic currents.

Materials and Methods

Ethical approval

All experiments were performed in accordance with the National Institutes of Health Guide for the Care and Use of Laboratory Animals and approved by the Institutional Animal Care and Use Committee at the Nihon University School of Dentistry (AP15D040). I declare the present experiments complied with the journal's ethical principles and their animal ethics check list. All efforts were made to minimize the number of animals used and their suffering.

Animals

I used a vesicular-GABA transporter (VGAT)-Venus line A transgenic rats (N = 92) of either sex, in which Venus, a fluorescent protein (Nagai et al., 2002), was co-expressed with VGAT and had fluorescent labelling of almost all cortical GABAergic cells (Uematsu et al., 2008). At postnatal days 1-2, all pups were anaesthetized with isoflurane (2-3%). One group received a subcutaneous injection of 50 µl of capsaicin (100 mg/kg; Wako, Osaka, Japan) dissolved in 1 part TWEEN 80 (Sigma-Aldrich, St. Louis, MO, USA), 1 part ethanol, and 8 parts saline at the base of the neck. The other group received the same volume of the vehicle (Sham). The pups were placed on the heating pad (Bio Research Center, Nagoya, Japan) set at 37 °C until recovery from anesthesia. They were weaned approximately at 3 postnatal weeks and maintained under conventional conditions (12 hr light/dark cycle). They had free access to food and drinking water. Although we set the end point when the weight was lost more than 10% within a week after the capsaicin/vehicle treatment, none of CAP and Sham lost their weight, and thus all the rats were used for experiments.

Behavioral test

Eye-wiping test (Welk et al., 1984) was used to estimate the effectiveness of the capsaicin treatment on C-fiber reduction at 20-30 d after birth. The capsaicin solution (0.01%) was made by diluting the stock solution involving 1% capsaicin, 10% ethanol, and 10% Tween 80 with saline (1:100). The capsaicin solution (~10 µl) was applied to the cornea, and the number of eye-wiping behavior was counted by visual inspection for

2 min. To evaluate the control, the same solution except for capsaicin was applied in the same manner. All behavioral tests were performed under blind conditions.

Immunohistochemistry

To evaluate the reduction of C-fibers by capsaicin injection, I performed the immunohistochemistry of CGRP in the trigeminal ganglion (TG). Both sides of TGs were dissected out after immersed in the same fixative for 4 h at 4 °C. Post fixed TGs were kept in 0.01 M phosphate buffered saline (PBS) containing 30% sucrose for 12 h for cryoprotection. The specimens were then embedded in Tissue-Tek (Sakura Finetek, Tokyo, Japan) at -20 °C. TGs were cut in the horizontal plane along the long axis of the ganglion at a thickness of 16 μm. For analysis, every 10th section (4 sections per a TG) was chosen in each rat. Sections were thaw-mounted onto MAS-coated Superfrost Plus microscope slides (Matsunami, Osaka, Japan) and dried overnight. To identify CGRP expression immunohistochemically in TG neurons, rabbit anti-CGRP antibody (1:100 in 0.01 M PBS, Abcam, Cambridge, USA) and Alexa Fluor 488-conjugated donkey anti-rabbit IgG (1:100 in 0.01 M PBS; Invitrogen, Eugene, USA) were used as primary and secondary antibodies, respectively.

The region of interest was set where the somata innervating the maxillary branch were involved (Fig. 1). The threshold of immunoreactivity was set at 2 times of the background.

Optical Imaging

I first performed *in vivo* optical imaging to confirm that the targeted region in the IC certainly responded to noxious stimuli as previously reported (Horinuki et al., 2015, Nakamura et al., 2015, Horinuki et al., 2016, Nakamura et al., 2016; Fujita et al., 2017).

Urethane (1.4 g/kg, i.p.) was used to anesthetize the animals (postnatal days 35-42) in combination with atropine methyl bromide (5 mg/kg). Body temperature was maintained at 37°C using a heating pad (BWT-100, Bio Research Center). Lidocaine (2% gel, AstraZeneca, Tokyo, Japan) was applied to the incision. After a craniotomy, the left IC and surrounding cortices were loaded with the voltage-sensitive dye RH1691 (1 mg/ml, Optical Imaging, New York, USA) for approximately 1 h. Fluorescent changes in RH1691 were measured by a charge-coupled device (CCD) camera

(MiCAM02, Brainvision, Tokyo, Japan) mounted on a stereomicroscope (Leica Microsystems, Wetzler, Germany). A tungsten-halogen lamp (CLS150XD, Leica Microsystems) illuminated the cortical surface through a 632-nm excitation filter and a dichroic mirror. The fluorescent emission was captured through an absorption filter (λ > 650-nm longpass, Andover, Salem, USA).

Bipolar enamel-coated copper wire electrodes (diameter = 100 μm; Tamagawadensen, Tokyo, Japan) were inserted into the pulp of the right maxillary first molar, and electrical stimulation was applied by five trains of voltage pulses (80 μs, 50 Hz, 5 V) at 20 s intervals using the electrical stimulator (STG2008, Multi Channel Systems, Reutlingen, Germany).

Values without stimuli were subtracted from each recording to remove signals caused by acute bleaching of the dye. The sampling interval was set at 4 ms. Twenty-four consecutive images responding to the stimuli were averaged to improve the signal-to-noise ratio.

Slice preparations

The techniques for preparing and maintaining rat cortical slices in vitro were similar to those described previously (Kobayashi et al., 2012; Koyanagi et al., 2014; Yamamoto et al., 2015; Kaneko et al., 2016; Yokota et al., 2016). Briefly, VGAT line A rats of either sex, aged from 20-30 days old, were deeply anaesthetized with isoflurane (5%; Pfizer, Tokyo, Japan) and decapitated. The brain including IC was rapidly removed and stored for 3 min in ice-cold, modified artificial cerebrospinal fluid (ACSF). The composition of the modified ACSF was as follows (in mM): 230 sucrose, 2.5 KCl, 10 $MgSO_4$, 1.25 NaH_2PO_4, 26 $NaHCO_3$, 0.5 $CaCl_2$, and 10 D-glucose. Coronal slices were cut at 350 μm thickness using a microslicer (LinearSlicer Pro 7, Dosaka EM, Kyoto, Japan). Slices were incubated at 32°C for 10 min in a submersion-type holding chamber filled with a normal ACSF (pH 7.35-7.40). The normal ACSF contained the following (in mM): 126 NaCl, 3 KCl, 2 $MgSO_4$, 1.25 $NaH_2 PO_4$, 26 $NaHCO_3$, 2 $CaCl_2$, and 10 D-glucose. The modified and normal ACSF were continuously aerated with a mixture of 95% O_2 / 5% CO_2. Then slices were maintained at room temperature until they were used for recording.

Cell identification and whole-cell patch-clamp recording

The slices were transferred to a recording chamber that was continuously perfused with the normal ACSF at a rate of 2.0-3.5 ml/min. Dual whole-cell patch-clamp recordings were obtained from Venus-positive fluorescent neurons and from Pyr identified in layers II/III using a fluorescence microscope equipped with Nomarski optics (BX51, Olympus, Tokyo, Japan) and an infrared-sensitive video camera (Hamamatsu Photonics, Hamamatsu, Japan). The distance between Venus-positive cells and Pyr was < 50 μm. Electrical signals were recorded by amplifiers (Axoclamp 700B, Molecular Devices, Sunnyvale, USA), digitized (Digidata 1440A, Molecular Devices), observed online, and stored on a computer hard disk using Clampex (pCLAMP 10, Molecular Devices).

The composition of the pipette solution for recordings from interneurons and Pyr was as follows (in mM): 85.4 potassium gluconate, 70 KCl, 10 HEPES, 0.5 EGTA, 2 $MgCl_2$, 2 ATP, and 0.3 GTP. The pipette solution had a pH of 7.3 and an osmolality of 300 mOsm. The liquid junction potential was -9 mV, and the voltage was not corrected. Thin-wall borosilicate patch electrodes (2-5 MΩ) were pulled on a Flaming-Brown micropipette puller (P-97, Sutter Instruments, Novato, USA). Recordings were obtained at 30-31°C. Seal resistance was > 5GΩ, and only data obtained from electrodes with access resistance of 6-20 MΩ and < 20% change during recordings were included in this study. Series resistance was 50% compensated. Membrane currents and potentials were low-pass filtered at 5-10 kHz and were digitized at 20 kHz.

Voltage responses of presynaptic and postsynaptic cells were recorded by applying long hyperpolarizing and depolarizing current pulse (300 ms) injections to examine basic electrophysiological properties including input resistance, single action potential kinetics, voltage-current relationship, and firing frequency. Because some cell pairs had mutual or greater than or equal to two connections, all cells were recorded under voltage-clamp conditions (holding potential -70 mV) during inhibitory postsynaptic current (IPSC) recordings.

IPSC recordings

Miniature IPSCs (mIPSCs) were recorded from Pyr and FS in IC layers II/III under application of 1 μM tetrodotoxin (TTX; Abcam, Cambridge, UK), 25 μM D-(-)-2-amino-5-phosphonopentanoic acid (D-APV, Abcam), and 20 μM

6,7-dinitroquinoxaline-2,3-dione (DNQX; Abcam). Before and after mIPSC recording, series resistance was measured to check recording condition.

Tonic currents mediated by extrasynaptic $GABA_A$ receptors were recorded under application of 25 μM D-APV and 20 μM DNQX. After recording the stable spontaneous currents, 100 μM picrotoxin, a noncompetitive $GABA_A$ receptor antagonist, was applied.

Paired depolarizing voltage-step pulses (2 ms, 80 mV) were applied at 50 ms interval to a presynaptic cell to induce action currents in the presynaptic cell and unitary IPSCs (uIPSCs) in a postsynaptic cell. Interstimulus interval between the paired-pulse stimulation was set at 0.1 Hz. Paired-pulse ratio (PPR) was obtained from the value of the second uIPSC amplitude divided by the first.

To evaluate the precise synaptic profiles including the number of release sites, release probability, and quantal content, I performed variance-mean (V-M) analysis (Silver et al., 1998; Foster and Regehr, 2004). In addition to the recording of uIPSCs under normal ASCF application, I recorded uIPSCs during changing $[Ca^{2+}]_o$ under application of different calcium concentrations (1, 2, and 4 mM) in ACSF. In this experiment, $[Mg^{2+}]_o$ was adjusted to keep the overall divalent cation concentration constant (4 mM). To avoid activating glutamatergic receptors, 20 μM DNQX and 25 μM D-APV were applied during recordings. Slices were perfused by the modified ACSFs for at least 10 min prior recording at each condition.

To estimate the quantal size of IPSCs in FS→Pyr connections, I further recorded uIPSCs under application of the ACSF in which $[Ca^{2+}]_o$ was replaced with 4 mM Sr^{2+}. Sr^{2+}-containing ACSF induces desynchronized GABA release, i.e. asynchronous IPSCs (aIPSCs), allowing the calculation of the quantal content of uIPSCs (Oliet et al., 1996; Bekkers and Clements, 1999). For aIPSC analysis, the first uIPSC (which is usually composed with less asynchronous currents) was discarded to reduce the influence of occasional multiquantal/nondesynchronized uIPSCs, and the subsequent aIPSCs were analyzed using a time window of 200 ms from the peak of the presynaptic action currents. To minimize a contamination of spontaneous IPSCs originating from other synapses, the time window for aIPSCs analysis was limited to 200 ms.

Data analysis

The optical imaging data were analyzed using Brain Vision Analyzer (Brain Vision LLC, Morrisville, NC, USA). Changes in the intensity of fluorescence (ΔF) in each pixel were divided by the initial intensity of fluorescence (F). The ratio (ΔF/F) was processed with a spatial filter (9 × 9 pixels). A significant response was defined as a signal that exceeded 9 times that of the standard deviation of the baseline noise.

The initial response was obtained by outlining the evoked excitation in the first frame that exhibited a significant increase in the optical signal. The maximum response was defined as the frame with the maximum amplitude of the optical signal in the center of excitation (Fig. 1). For the quantitative analysis of the spatiotemporal profiles of excitation, I measured the area of the maximum response and the amplitude, latency, 20-80% rise time, and half duration of the signals at the center of the initial response.

Clampfit (pClamp 10; Molecular Devices) was used to analyze current and voltage responses. Input resistance was measured from slopes of least-squares regression lines fitted to voltage–current curves measured at the peak voltage deflection (current pulse amplitude up to -100 pA). The amplitude of the action potential was measured from the resting membrane potential to the peak. By application of depolarizing step current pulses (300 ms), repetitive firing was evaluated from the slope of least-squares regression lines in a plot of the number of spikes versus the amplitude of injected current, i.e. frequency-current curve (up to approximately 450 pA).

The amplitudes of the uIPSCs were measured as the difference between peak postsynaptic currents and baseline currents taken from a 2-3 ms time window close to the onset of the current. To measure the 20-80% rise time and decay time constants of uIPSCs, 10 postsynaptic events were aligned to the peak of presynaptic action currents and averaged. The decay phase of uIPSCs was well fitted by a double exponential function as follows (Bacci et al., 2003):

$$f(t) = A_{fast} \exp(-t/\tau_{fast}) + A_{slow} \exp(-t/\tau_{slow}) . \quad (1)$$

where A_{fast} and A_{slow} are the amplitudes of fast and slow decay components, respectively, and τ_{fast} and τ_{slow} are their respective decay time constants. The weighted decay time constant (τ_w) was calculated using the following equation (Bacci et al. 2003):

$$\tau_w = [(A_{fast}\tau_{fast}) + (A_{slow}\tau_{slow})] / (A_{fast} + A_{slow}) . \quad (2)$$

mIPSCs were detected at a threshold of 3× the standard deviation of the baseline noise amplitude using event detection software (kindly provided by Prof. John Huguenard, Stanford University). To measure the amplitude and inter-event interval, mIPSCs were analyzed from continuous 5-7 min recordings. Consecutive 100 events were picked from each neuron and summed to obtain cumulative plots of the inter-event interval and the amplitude of mIPSCs. The amplitude and inter-event interval of mIPSCs were also evaluated by averaging each value.

The amplitude of tonic currents was obtained by subtracting the holding currents before and after application of picrotoxin, which completely abolished spontaneous IPSCs.

The variance-mean (V-M) analysis was performed as previously described (Silver et al. 1998; Foster and Regehr, 2004) to evaluate the number of release sites, release probability, and quantal content. I obtained 20-40 uIPSCs in each Ca^{2+} concentration (2, 4, 1 mM), and the mean uIPSC amplitude (*M*) was calculated and plotted against their varience (*V*). Individual plots were fitted with a quadratic equation assuming zero variance at zero amplitude. The quantal content (*q*) and number of release sites (*N*) were estimated by expressing the equation as follows:

$$V = qM - M^2/N. \quad (3)$$

The release probability (*Pr*) was estimated by the equation as follows:

$$Pr = M/qN, \quad (4)$$

where *M* is divided by the product of the quantal content (*q*) and number of release sites (*N*).

Statistics

Data are presented as the mean ± standard error of the mean. The number of animals and pair of neurons are expressed as N and n, respectively. The density of CGRP-immunopositive neurons between CAP and Sham was compared by Student's *t*-test. Student's *t*-test with Bonferroni correction was used to compare the frequency of eye-wiping responding to vehicle or capsaicin in CAP and Sham. Comparisons of uIPSC amplitude, PPR, and mIPSC amplitude and the inter-event interval between CAP and Sham were conducted using Student's *t*-tests. In the cases without normal distributions and equal variances, Mann-Whitney *U* test was used for the comparisons.

In this case, data are presented as the median. Cumulative probability distributions of the amplitude and inter-event interval of mIPSCs and aIPSCs were analyzed using the non-parametric Kolmogorov-Smirnov test to evaluate the significant differences between CAP and Sham. $P < 0.05$ was considered to indicate statistically significant.

Results

Before testing electrophysiological profiles of IC neurons in CAP and Sham, I evaluated the number of C-fibers in CAP by CGRP immunohistochemistry, which clarifies TRPV1-immunopositive neurons in TG. In addition, eye-wiping test was performed to confirm that reduction of the density of CGRP-immunopositive cells in TG of CAP definitely affects the sensitivity to capsaicin. After investigating the effectiveness of capsaicin treatment, whole-cell patch-clamp analyses were performed to examine changes of intrinsic and inhibitory synaptic properties in CAP and Sham.

CGRP immunohistochemistry

It is known that capsaicin is a selective agonist to TRPV1, which induces selective reduction of unmyelinated fiber expressing the receptor. The number of CGRP-immunopositive neurons in the TG is reliable to evaluate the reduction of TRPV1 (Wimalawansa, 1993; Cavanaugh et al., 2009). Therefore, to estimate the loss of C-fibers in CAP, CGRP-immunohistochemistry was examined at postnatal days 20-30, when the electrophysiological experiments were performed.

TG in CAP showed the less number of CGRP-immunopositive cells comparing to that in Sham (Fig. 1B). The loss of CGRP-positive cells occurred in any regions that involve somata innervating the first, second, and third branches of the trigeminal nerve, suggesting that the capsaicin treatment elicited non-specific loss of the peripheral neurons. In the present study, the density of CGRP-immunopositive neurons was measured in the region of the second branch (see Materials and Methods; Fig. 1A). The number of CGRP-immunopositive neurons was 48.4 ± 4.0 cell/mm^2 in CAP (N = 21) and 91.7 ± 15.8 cell/mm^2 in Sham (N = 14), indicating a significant decrease in the number of CGRP-positive neurons in CAP ($t(33) = 3.32$, $P < 0.001$; Student's t-test; Fig. 1C) and strongly suggesting a significant loss of C-fibers in CAP.

Behavioral test

Sham showed frequent eye-wiping (23.5 ± 1.5 per 2 min, N = 10) to 10 μl vehicle application to their eyes, whereas a droplet of capsaicin solution (0.01% in vehicle, 10 μl) to their eyes induced much higher frequency of eye-wiping (72.6 ± 2.8 per 2 min, N

= 10; $t(18) = 16.3$, $P < 0.01$, Student's *t*-test with Bonferroni correction; Fig. 1D). On the other hand, CAP showed a similar frequency of eye-wiping responding to the vehicle droplet (21.9 ± 1.4 per 2 min, N = 9) and to the capsaicin droplet (22.0 ± 2.5 per 2 min, N = 9) in comparison to that of vehicle application in Sham ($t(18) = 0.815$, $P = 0.27$, Student's *t*-test with Bonferroni correction; Fig. 1D). The frequency of eye-wiping to vehicle in CAP was comparable to that in Sham (Fig. 1D). These results suggest that capsaicin treatment induces a significant loss of C-fibers.

Optical imaging

The IC is a rostrocaudally longitudinal strip lying on the dorsal bank of the rhinal fissure, and receives different sensory inputs depending on the subdivision of the IC (Kobayashi, 2011). Therefore, I first identified the region of the IC responding to noxious inputs from the orofacial area by optical imaging in CAP and in Sham.

In accordance with previous studies (Nakamura et al., 2015, 2016), the dorsal part of the IC caudally adjacent to the middle cerebral artery invariably responded to the electrical stimulation of the upper molar pulp in Sham (Fig. 1E). The CAP also showed that the similar IC region was excited by noxious stimuli (Fig. 1E). Fig. 1F shows the superimposed images of the maximum excitatory propagation in CAP (N = 5) and Sham (N = 6). Although the CAP exhibited larger excitatory area of the maximum response than Sham (29.6 mm^2, N = 5, in CAP and 25.5 mm^2, N = 6, in Sham; Mann-Whitney *U* test, $t(9) = 42.0$, $P < 0.05$; Fig. 1G), the dorsal IC caudally adjacent to the middle cerebral artery was commonly activated by electrical stimulation of the molar pulp, indicating this region of the IC receives noxious inputs both in CAP and Sham.

The peak amplitude of excitation in CAP (0.83 ± 0.10, N = 5) was significantly larger than that in Sham (0.51 ± 0.07, N = 6; Student's *t*-test, $t(9) = 2.37$, $P < 0.05$; Fig. 1H), suggesting that the cortical excitation induced by dental pulp stimulation is facilitated in CAP. On the other hand, the latency of IC excitation in CAP (14 ms, N = 5) was comparable to that in Sham (14 ms, N = 6; Mann–Whitney *U* test, $t(9) = 28.0$, $P = 0.792$; Fig. 1H). CAP showed similar 20-80% rise time (8 ms, N = 5) and 80-20% decay time (92.8 ± 14.9 ms, N = 5) to those of Sham (4 ms, N = 6 in rise time; Mann–Whitney *U* test, $t(9) = 36.5$, $P = 0.247$; 128.7 ± 20.9 ms, N = 6 in decay time; Student's *t*-test, $t(9) = 1.21$, $P = 0.255$; Fig. 1H).

In reference to the results obtained from the optical imaging experiment, the following patch-clamp experiments were performed using the coronal slice preparation obtained from the IC 0-1050 μm caudally from the middle cerebral artery (Fig. 1F).

Effects of capsaicin treatment on basic membrane properties

Paired whole-cell patch-clamp recordings were performed from Venus-positive GABAergic cells and Venus-negative Pyr in layers II/III of IC. Venus-positive cells in IC were classified into FS and other GABAergic neurons including low threshold spike and late-spiking cells as previously reported (Koyanagi et al., 2010; Yamamoto et al., 2010; Kobayashi et al., 2012). To examine the effects of capsaicin treatment on inhibitory neural circuits in IC, FS→Pyr connections were focused because FS occupy a major part of GABAergic interneurons and provide powerful inhibition to somata and proximal dendrites of Pyr in the cerebral cortex (Hu et al., 2014).

FS was characterized by repetitive spike firing responding to a long depolarizing current pulse injection at extremely high frequency without spike adaptation (Fig. 3A, B and Fig. 5A,B). In addition, action potential of FS showed short duration with deep afterhyperpolarization in comparison to that of Pyr. Table 1 summarizes the firing properties of Pyr and FS in CAP and Sham. There were little changes between CAP and Sham both in Pyr and FS electrophysiological properties, including the resting membrane potential, input resistance, and spike and repetitive firing properties (Student's *t*-test).

Miniature IPSCs in pyramidal neurons

To examine whether the GABAergic synaptic input is altered by capsaicin treatment in the neonatal period, I first measured the amplitude and inter-event interval of mIPSCs from Pyr under bath application of 1 μM TTX, 25 μM D-APV, and 20 μM DNQX in CAP (N = 10) and Sham (N = 14; Fig. 2).

CAP showed smaller amplitude of mIPSCs in Pyr (16.0 ± 1.3 pA, n = 16) than Sham (21.0 ± 1.0 pA, n = 19; $t(33) = 3.23$, $P < 0.01$, Student's *t*-test; Fig. 2C,D,G). The cumulative probability of mIPSC amplitude obtained from 16 Pyr in CAP and 19 Pyr in Sham (see Experimental Procedures) indicated smaller amplitudes of mIPSCs in CAP compared to that in Sham ($P < 0.01$, Kolmogorov-Smirnov test; Fig. 2E). In contrast,

there was no significant difference in the inter-event interval of mIPSC in Pyr: 0.69 ± 0.08 s in CAP (n = 16) versus 0.66 ± 0.06 s in Sham (n = 19; $t(33) = 0.268$, $P = 0.80$, Student's *t*-test; Fig. 2C,D,H). The cumulative probability of mIPSC inter-event interval obtained from 16 Pyr in CAP and 19 Pyr in Sham also showed about the same inter-event interval in CAP compared to that in Sham ($P = 0.07$, Kolmogorov-Smirnov test; Fig. 2F). These data indicate that capsaicin treatment reduces mIPSC amplitude in a postsynaptic manner in Pyr. Moreover, I recorded mIPSC from FS of CAP and Sham and evaluated the amplitude and inter-event interval of mIPSC. The amplitude of mIPSC in CAP (17.7 ± 1.6 pA, n =18) showed a significant decrease compared with that in Sham (22.2 ± 1.5 pA, n = 11; $t(27) = 2.21$, $P < 0.05$, Student's *t*-test; Fig. 3C,D,E). On the other hand, there were little difference between CAP and Sham in the inter-event interval of the mIPSC (CAP: 0.77 ± 0.07 s, n = 18; Sham: 0.91 ± 0.19 s, n = 11, $t(27) = 0.77$, $P = 0.45$, Student's *t*-test; Fig. 3C,D,F). Thus, FS also received smaller mIPSC amplitude in CAP than that in sham may be because of postsynaptic changes in FS.

To record tonic currents that were induced by extrasynaptic $GABA_A$ receptor activation, I applied 25 μM D-APV and 20 μM DNQX and recorded spontaneous IPSCs (Fig. 4A,B). Picrotoxin (100 μM) was then added to block $GABA_A$ receptors. Picrotoxin completely diminished spontaneous IPSCs (Fig. 4A,B). The holding currents before and after application of picrotoxin were subtracted to obtain the tonic current. The amplitude of tonic current recorded from Pyr in CAP (8.9 ± 5.6 pA, n = 13, N = 3) was comparable to that in Sham (9.1 ± 3.6 pA, n = 17, N = 3; $t(28) = 0.029$, $P = 0.98$, Student's *t*-test; Fig. 4C), suggesting that extrasynaptic $GABA_A$ receptors have little effect by capsaicin treatment.

Unitary IPSCs obtained from FS→Pyr connections

Heterogeneous GABAergic interneurons contribute to the induction of mIPSCs in IC (Koyanagi et al., 2010). Therefore, smaller amplitudes of mIPSCs might be due to the reduction of IPSC amplitude from FS but not from non-FS to Pyr connections. Another possibility is that hyperactivation of low threshold spike cells, which induces smaller amplitude of IPSCs than FS (Koyanagi et al., 2010), and depression of IPSC frequency in FS→Pyr connections might occur in CAP. Alternatively, a depression of postsynaptic

$GABA_A$ receptors may result in a decrease in the mIPSC amplitude. Multiple whole-cell recording, which can identify presynaptic neuron subtypes, has an advantage to clarify this point, and therefore, I subsequently focused on FS→Pyr connections and recorded uIPSCs by paired whole-cell patch-clamp recording (Fig. 5).

The most profiles of uIPSCs in CAP (N = 9) were almost comparable to those in Sham (N = 6). The rise time from 20% to 80% in uIPSC amplitude were 0.75 ± 0.06 ms in CAP (n = 22) and 0.64 ± 0.04 ms in Sham (n = 11, $t(31) = 1.39$, $P = 0.09$, Student's *t*-test). The decay time constant (τ_w; see Materials and Methods) in CAP was 17.9 ± 2.8 ms (n = 22), which was also comparable to that in Sham (14.8 ± 1.4 ms, n = 11, $t(31) = 1.24$, $P = 0.28$, Student's *t*-test). Moreover, PPR, which reflects the release probability of synaptic vesicle from the presynaptic terminals (Debanne et al., 1996), in CAP (0.72 ± 0.06, n = 21) was comparable to that in Sham (0.66 ± 0.04, n = 14; $t(33) = 0.902$, $P = 0.63$, Student's *t*-test; Fig. 5F). On the other hand, the amplitude of uIPSCs obtained from CAP (91.7 ± 30.2 pA, n = 21) was smaller than that from Sham (186.0 ± 30.8 pA, n = 14; $t(33) = 3.07$, $P < 0.05$, Student's *t*-test; Fig. 5C-E).

Malinow and Tsien (1990) reported the inverse of the squared coefficient of variation ($1/CV^2$) of the amplitude is the index for presynaptic mechanisms including the release probability and the number of release sites. There was no significant difference in $1/CV^2$ between CAP and Sham (CAP, 9.0 ± 1.9, n = 21; Sham, 11.9 ± 3.0, n = 14; $t(33) = 0.898$, $P = 0.43$, Student's *t*-test; Fig. 5G). These results indicate that the different kinetics of uIPSCs in FS→Pyr connections of CAP are likely to be induced not by presynaptic but by postsynaptic mechanisms.

Asynchronous IPSCs in FS→Pyr connections

Replacing Ca^{2+} to Sr^{2+} induces asynchronous release of GABA from presynaptic terminals, which is considered to induce IPSCs in a quantal unit (Oliet et al., 1996; Bekkers and Clements, 1999). By applying this method to uIPSC recording from FS→Pyr connections, I evaluated IPSCs that are elicited by quantal release of GABA from FS terminals (Fig. 6). To lessen the contamination of spontaneous IPSCs, I set the time window of aIPSC analysis from the stimulus artifact to 200 ms, discarding the first aIPSC, which highly involved multiquantal and/or nondesynchronized uIPSCs.

The replacement of Ca^{2+} with Sr^{2+} gradually reduced uIPSC amplitude with an increase in the number of aIPSCs with small amplitude following the first uIPSCs (Fig. 6A-D). The cumulative plot of aIPSC amplitude also indicated the smaller amplitude in CAP ($P < 0.001$, Kolmogorov-Smirnov test; Fig. 6E). The amplitude of aIPSCs in CAP (16.1 ± 0.9 pA, n = 6, N = 6) was smaller than that in Sham (22.8 ± 1.5 pA, n = 6, N = 6; $t(10) = 4.79$, $P < 0.05$, Student's *t*-test; Fig. 6F). The amplitude of aIPSCs of CAP and Sham were comparable to those of mIPSCs as shown in Fig. 2 ($t(20) = 0.064$, $P = 0.94$, Student's *t*-test), supporting the idea that aIPSCs are induced by quantal release of GABA. On the other hand, no significant difference in the frequency of aIPSCs in the analyzed time window was observed between the two groups (CAP, 4.8 ± 0.7 Hz, n = 6; Sham, 4.7 ± 1.1 Hz, n = 6; $t(10) = 0.128$, $P = 0.90$, Student's *t*-test). These results supported the proposed idea described above that CAP shows smaller IPSCs than those of Sham via postsynaptic mechanisms.

Variance-mean analysis of uIPSCs

The reduction of uIPSC and aIPSC amplitude without changes in the mIPSC frequency and PPR suggesting a smaller quantal size (*q*) rather than presynaptic changes in CAP. To confirm this hypothesis, I employed V-M analysis and evaluated three parameters of synaptic function; *q*, release probability (*Pr*), and the number of release site (*N*) in FS→Pyr connections of CAP (N = 8) and Sham (N = 8; Fig. 7).

During continuous uIPSC recording from FS→Pyr connections, the concentrations of 1.0, 2.0, and 4.0 mM $[Ca^{2+}]_o$ were used in order to alter the release probability (Fig. 7A-D). The variance was calculated from 30-50 traces at each epoch and plotted against the averaged amplitude of the respective uIPSCs (Fig. 7A-D). By fitting the plots with second-degree polynomial equation, putative *Pr*, *N* and *q* were obtained from each neuron (Fig. 7E,F). Smaller *q* was detected in CAP (20.3 ± 3.7, n = 14) than Sham (34.3 ± 6.0, n = 10; $t(22) = 2.72$, $P < 0.05$, Student's *t*-test; Fig. 7G). On the other hand, *Pr* in CAP (0.36 ± 0.05, n = 14) was similar to that in Sham (0.34 ± 0.08, n = 10; $t(22) = 0.298$, $P = 0.78$, Student's *t*-test; Fig. 7H). Similar to *Pr*, *N* was comparable between CAP (19.2 ± 4.1, n = 14) and Sham (25.8 ± 9.6, n = 10; $t(22) = 0.738$, $P = 0.48$, Student's *t*-test; Fig. 7I). These results strongly suggest the possibility that reduction of

C-fibers by injection of capsaicin in the neonatal period depresses q in FS→Pyr connections of IC.

Discussion

Reduction of primary afferent C-fibers in CAP was confirmed by loss of immunolabelling CGRP-positive neurons in TG and reduced frequency of eye-wiping. Reduction of amplitudes in both mIPSC and uIPSC were observed in CAP. The small quantal content of GABAergic transmission was detected by V-M analysis and aIPSC recorded under replacement of extracellular Ca^{2+} with Sr^{2+}, and the mechanisms of IPSC depression was likely to be postsynaptic modulation. These findings are along the same lines in other sensory cortices that plastic changes of GABAergic synapses by disturbing sensory inputs, and extends them by demonstrating that plastic changes in IC by C-fiber afferent reduction are controlled by postsynaptic mechanisms.

C-fiber reduction induces plastic changes in inhibitory synaptic transmission in IC

The GABAergic system of the cerebral cortex plays a key role in the regulation of changes in the local cortical circuits due to disturbances of sensory inputs (see review by Hensch, 2005). The present results of a decrease in GABAergic synaptic transmission corroborate this hypothesis: sensory disturbance, in the present case, deletion of C-fibers, influences GABAergic synaptic transmission.

The suppressed IPSCs mediated by $GABA_A$ receptors in CAP may induce hyperexcitation of IC activity, because cortical excitatory neurons including Pyr receive dense GABAergic inhibitory synaptic inputs. Indeed, *in vivo* optical imaging revealed the facilitated excitatory propagation in the IC and adjacent somatosensory cortex responding to dental pulp stimulation in CAP. This result might suggest that nociceptive inputs primarily transmitted by Aδ-fibers are processed with intensified attention in IC of CAP. Eye wiping reflex by capsaicin application to the cornea of CAP was comparable to that by vehicle application in CAP and Sham, suggesting less possibility of firing alteration of Aδ-fibers. Rather, the noxious information processing is likely to be enhanced in the higher brain regions including the thalamus and IC.

In addition to GABAergic synaptic transmission, sensory deprivation induces plastic changes in the intrinsic neural properties in principal neurons, regular-spiking nonpyramidal neurons, and FS in the sensory cortex (Maffei et al., 2004; Xu et al., 2007; Sun, 2009). In contrast to these studies, the present results demonstrate a lesser

effect of C-fiber deletion on both Pyr and FS. This suggests that not all disturbance of sensory inputs induce intrinsic plasticity in the cerebral cortex. Stimulation of Aδ- and C-fibers is likely to elicit action potential in a different temporal manner: Aδ-fibers are activated rapidly responding to stimuli, i.e., fast pain, whereas C-fibers show sustained activities with longer latency (slow pain). These profiles are characteristic to nociception and not adaptable to visual, auditory, and whisker sensation and such temporal differences might be a reason for inconsistent sensitivity of intrinsic plasticity between IC and other sensory cortices.

Synaptic mechanisms of the reduction of IPSCs

To evaluate the synaptic mechanisms for the changes in inhibitory synaptic transmission mediated by $GABA_A$ receptors, multiple approaches were employed: mIPSC, uIPSC, and aIPSC recordings. Reduction of mIPSC amplitude without a difference in the inter-event interval suggests that there are postsynaptic changes in CAP. This hypothesis was consistently supported by the reduced amplitude of aIPSCs, the reduced amplitude of uIPSCs without changing PPR, and the decrease in q revealed by V-M analysis.

There are several possible mechanisms for the reduction of the amplitude of IPSCs via postsynaptic changes. The first is a switch of $GABA_A$ receptor subunits. $GABA_A$ receptor is a pentamer composed of α1-6, β1-4, γ1-4, δ, ε, π, and θ subunits, and in the central nervous system, α, β, and γ are dominant subunits (Cherubini and Conti, 2001). Several subunits play critical roles in regulating decay kinetics of IPSCs, which affect the amplitude of IPSCs in the cortical neurons. IPSCs via α1 subunit-containing $GABA_A$ receptors exhibit faster decay kinetics than those with α3 subunit (Bosman et al., 2002; Bacci et al., 2003; Li et al., 2009). Moreover, in the reticular thalamic neurons, β1 subunits are expressed with rapid decay kinetics of sIPSCs (Huntsman and Huguenard, 2006). However, the present study demonstrated no different decay kinetics of IPSCs between CAP and Sham, suggesting that this possibility does not fit to the present case.

Second, phosphorylation of $GABA_A$ receptors possibly changes the IPSC amplitude. Indeed, cultured cortical neurons expressing β3 subunits show protein kinase C-dependent phosphorylation, which reduces GABAergic currents (Brandon et al.,

2000). IPSCs recorded from hippocampal neurons are also sensitive to protein kinases A and C: protein kinase A reduces mIPSC conductance in CA1 Pyr, whereas protein kinase C enhances mIPSCs in dentate granule cells with changes in decay kinetics (Poisbeau et al., 1999). Although changes in phosphorylation of $GABA_A$ receptors might occur in CAP, the consistent decay kinetics in CAP suggest that the second possibility is also unlikely.

The third and the most probable mechanism is a reduction of the number of $GABA_A$ receptors expressed in the postsynaptic membrane. The plastic change in q is reported in several regions of the cortex, i.e., the visual (Morales et al., 2002) and auditory cortex (Kotak et al., 2008).

C-fiber deletion by capsaicin treatment

Systemic injection of capsaicin has been used to specifically ablate C-fibers (Holzer, 1991). Capsaicin activates TRPV1 receptor, a nonselective cation channel, expressed in the peripheral nerves, and induces depolarization by cation influx (Bevan and Szolcsanyi, 1990). In the neonatal period, injection of capsaicin induces large depolarization, which in turn causes cell death (Bevan and Szolcsanyi, 1990). As the expression of TRPV1 receptors is higher in C-fibers than Aδ-fibers, C-fibers are selectively deleted (Caterina and Julius, 2001). The present results of the behavioral experiment indicate that this is the case in the trigeminal nerves.

Although capsaicin treatment reduces C-fibers in the peripheral nerves, I must take into consideration that neurons in the central nervous systems also express TRPV1 receptors (Beggs et al., 2010), and therefore, injection of capsaicin may not only act on the peripheral nerves, including the trigeminal system but also on the central nervous system. The latter influence might induce the changes in FS→Pyr connections of IC. This issue should be further examined in the future.

Functional implication

Both fast and slow pain, which are mediated by Aδ- and C-fibers, are likely to be processed in IC (Nakamura et al., 2015), though the mechanisms for nociceptive information processing of these different modalities have been unknown. The present study demonstrated that reduction of C-fibers induced plastic changes in inhibitory

synaptic transmission in IC. This finding could be evidence that the pathways of Aδ- and C-fiber-mediated nociception interact with each other in IC rather than being parallel or independent. It might be a reasonable speculation that a part of neurons receives competitive inputs from both Aδ- and C-fiber-mediated pathways (Ohara et al., 2005; Todd, 2010). If that is the case, loss of C-fiber inputs may increase inputs from Aδ-fibers, and a depression of inhibitory inputs to Pyr, based on the present results, may contribute to this alteration of the cortical circuit.

The reduction of uIPSCs may result in facilitating the activities of Pyr, even though the number of C-fibers is reduced. Less nociceptive inputs may act as a booster of excitation via this mechanism (i.e. less inhibition), to maintain the IC response to noxious inputs. The facilitative excitation in IC may maintain the sensitivity to nociceptive inputs that are partially disturbed by C-fiber deletion.

Acknowledgements

VGAT-Venus transgenic rats were generated by Drs. Y. Yanagawa, M. Hirabayashi and Y. Kawaguchi in the National Institute for Physiological Sciences, Okazaki, Japan, using pCS2-Venus provided by Dr. A. Miyawaki. I thank Prof. Noriaki Koshikawa for his critical reading of the manuscript and Dr. Asako Kubo for her kind instruction for making the model animals.

References

Bacci A, Rudolph U, Huguenard JR, Prince DA (2003). Major differences in inhibitory synaptic transmission onto two neocortical interneuron subclasses. J Neurosci 23: 9664-9674.

Beggs S, Liu XJ, Kwan C, Salter MW (2010). Peripheral nerve injury and TRPV1-expressing primary afferent C-fibers cause opening of the blood-brain barrier. Mol Pain 6: 74.

Bekkers JM, Clements JD (1999). Quantal amplitude and quantal variance of strontium-induced asynchronous EPSCs in rat dentate granule neurons. J Physiol 516: 227-248.

Bevan S, Szolcsányi J (1990). Sensory neuron-specific actions of capsaicin: mechanisms and applications. Trends Pharmacol Sci 11: 330-333.

Bliss TV, Collingridge GL, Kaang BK, Zhuo M (2016). Synaptic plasticity in the anterior cingulate cortex in acute and chronic pain. Nat Rev Neurosci 17: 485-496.

Bosman LW, Rosahl TW, Brussaard AB (2002). Neonatal development of the rat visual cortex: synaptic function of $GABA_A$ receptor alpha subunits. J Physiol 545: 169-181.

Brandon NJ, Delmas P, Kittler JT, McDonald BJ, Sieghart W, Brown DA, Smart TG, Moss SJ (2000). $GABA_A$ receptor phosphorylation and functional modulation in cortical neurons by a protein kinase C-dependent pathway. J Biol Chem 275: 38856-38862.

Caterina MJ, Julius D (2001). The vanilloid receptor: a molecular gateway to the pain pathway. Annu Rev Neurosci 24: 487-517.

Cavanaugh DJ, Lee H, Lo L, Shields SD, Zylka MJ, Basbaum AI, Anderson DJ (2009). Distinct subsets of unmyelinated primary sensory fibers mediate behavioral responses to noxious thermal and mechanical stimuli. Proc Natl Acad Sci USA 106: 9075-9080.

Cherubini E, Conti F (2001). Generating diversity at GABAergic synapses. Trends Neurosci 24: 155-162.

Debanne D, Guérineau NC, Gähwiler BH, Thompson SM (1996). Paired-pulse facilitation and depression at unitary synapses in rat hippocampus: quantal fluctuation affects subsequent release. J Physiol 491: 163-176.

Foster KA, Regehr WG (2004). Variance-mean analysis in the presence of a rapid

antagonist indicates vesicle depletion underlies depression at the climbing fiber synapse. Neuron 43: 119-131.

Fujita S, Kaneko M, Nakamura H, Kobayashi M (2017). Spatiotemporal profiles of proprioception processed by the masseter muscle spindles in rat cerebral cortex: an optical imaging study. Front Neural Circuit 11: 4.

Gogolla N, Takesian AE, Feng G, Fagiolini M, Hensch TK (2014). Sensory integration in mouse insular cortex reflects GABA circuit maturation. Neuron 83: 894-905.

Hensch TK (2005). Critical period mechanisms in developing visual cortex. Curr Top Dev Biol 69: 215-237.

Holzer P (1991). Capsaicin: cellular targets, mechanisms of action, and selectivity for thin sensory neurons. Pharmacol Rev 43: 143-201.

Horinuki E, Shinoda M, Shimizu N, Koshikawa N, Kobayashi M (2015). Orthodontic force facilitates cortical responses to periodontal stimulation. J Dent Res 94: 1158-1166.

Horinuki E, Yamamoto K, Shimizu N, Koshikawa N, Kobayashi M (2016). Sequential changes in cortical excitation during orthodontic treatment. J Dent Res 95: 897-905.

Hu H, Gan J, Jonas P (2014). Fast-spiking, parvalbumin^{+} GABAergic interneurons: from cellular design to microcircuit function. Science 345: 6196, 1255263.

Huntsman MM, Huguenard JR (2006). Fast IPSCs in rat thalamic reticular nucleus require the $GABA_A$ receptor β_1 subunit. J Physiol 572: 459-475.

Iwai Y, Fagiolini M, Obata K, Hensch TK (2003). Rapid critical period induction by tonic inhibition in visual cortex. J Neurosci 23: 6695-6702.

Kaneko K, Koyanagi Y, Oi Y, Kobayashi M (2016). Propofol-induced spike firing suppression is more pronounced in pyramidal neurons than in fast-spiking neurons in the rat insular cortex. Neuroscience 339: 548-560.

Kobayashi M (2011). Macroscopic connection of rat insular cortex: anatomical bases underlying its physiological functions. Int Rev Neurobiol 97: 285-303.

Kobayashi M, Takei H, Yamamoto K, Hatanaka H, Koshikawa N (2012). Kinetics of $GABA_B$ autoreceptor-mediated suppression of GABA release in rat insular cortex. J Neurophysiol 107: 1431-1442.

Kotak VC, Takesian AE, Sanes DH (2008). Hearing loss prevents the maturation of GABAergic transmission in the auditory cortex. Cereb Cortex 18: 2098-2108.

Koyanagi Y, Oi Y, Yamamoto K, Koshikawa N, Kobayashi M (2014). Fast-spiking cell

to pyramidal cell connections are the most sensitive to propofol-induced facilitation of GABAergic currents in rat insular cortex. Anesthesiology 121: 68-78.

Koyanagi Y, Yamamoto K, Oi Y, Koshikawa N, Kobayashi M (2010). Presynaptic interneuron subtype- and age-dependent modulation of GABAergic synaptic transmission by beta-adrenoceptors in rat insular cortex. J Neurophysiol 103: 2876-2888.

Kuner R, Flor H (2016). Structural plasticity and reorganisation in chronic pain. Nat Rev Neurosci 18: 20-30.

Li P, Rudolph U, Huntsman MM (2009). Long-term sensory deprivation selectively rearranges functional inhibitory circuits in mouse barrel cortex. Proc Natl Acad Sci USA 106: 12156-12161.

Maffei A, Nelson SB, Turrigiano GG (2004). Selective reconfiguration of layer 4 visual cortical circuitry by visual deprivation. Nature Neuroscience 7: 1353-1359.

Malinow R, Tsien RW (1990). Presynaptic enhancement shown by whole-cell recordings of long-term potentiation in hippocampal slices. Nature 346: 177-180.

Morales B, Choi SY, Kirkwood A (2002). Dark rearing alters the development of GABAergic transmission in visual cortex. J Neurosci 22: 8084-8090.

Nagai T, Ibata K, Park ES, Kubota M, Mikoshiba K, Miyawaki A (2002). A variant of yellow fluorescent protein with fast and efficient maturation for cell-biological applications. Nat Biotechnol 20: 87-90.

Nagy JI, Iversen LL, Goedert M, Chapman D, Hunt SP (1983). Dose-dependent effects of capsaicin on primary sensory neurons in the neonatal rat. J Neurosci 3: 399-406.

Nakamura H, Kato R, Shirakawa T, Koshikawa N, Kobayashi M (2015). Spatiotemporal profiles of dental pulp nociception in rat cerebral cortex: An optical imaging study. J Comp Neurol 523: 1162-1174.

Nakamura H, Shirakawa T, Koshikawa N, Kobayashi M (2016). Distinct excitation to pulpal stimuli between somatosensory and insular cortices. J Dent Res 95: 180-187.

Ohara PT, Vit JP, Jasmin L (2005). Cortical modulation of pain. Cellular and molecular life sciences : CMLS 62: 44-52.

Oliet SH, Malenka RC, Nicoll RA (1996). Bidirectional control of quantal size by synaptic activity in the hippocampus. Science 271: 1294-1297.

Poisbeau P, Cheney MC, Browning MD, Mody I (1999). Modulation of synaptic $GABA_A$ receptor function by PKA and PKC in adult hippocampal neurons. J

Neurosci 19: 674-683.

Remple MS, Henry EC, Catania KC (2003). Organization of somatosensory cortex in the laboratory rat (Rattus norvegicus): Evidence for two lateral areas joined at the representation of the teeth. J Comp Neurol 467: 105-118.

Silver RA, Momiyama A, Cull-Candy SG (1998). Locus of frequency-dependent depression identified with multiple-probability fluctuation analysis at rat climbing fiber-Purkinje cell synapses. J Physiol 510: 881-902.

Sun QQ (2009). Experience-dependent intrinsic plasticity in interneurons of barrel cortex layer IV. J Neurophysiol 102: 2955-2973.

Todd AJ (2010). Neuronal circuitry for pain processing in the dorsal horn. Nat Rev Neurosci 11: 823-836.

Uematsu M, Hirai Y, Karube F, Ebihara S, Kato M, Abe K, Obata K, Yoshida S, Hirabayashi M, Yanagawa Y, Kawaguchi Y (2008). Quantitative chemical composition of cortical GABAergic neurons revealed in transgenic venus-expressing rats. Cereb Cortex 18: 315-330.

Welk E, Fleischer E, Petsche U, Handwerker HO (1984). Afferent C-fibers in rats after neonatal capsaicin treatment. Pflugers Arch 400: 66-71.

Wimalawansa SJ (1993). The effects of neonatal capsaicin on plasma levels and tissue contents of CGRP. Peptides 14: 247-252.

Xu H, Kotak VC, Sanes DH (2007). Conductive hearing loss disrupts synaptic and spike adaptation in developing auditory cortex. Journal of Neuroscience 27: 9417-9426.

Yamamoto K, Koyanagi Y, Koshikawa N, Kobayashi M (2010). Postsynaptic cell type-dependent cholinergic regulation of GABAergic synaptic transmission in rat insular cortex. J Neurophysiol 104: 1933-1945.

Yamamoto K, Takei H, Koyanagi Y, Koshikawa N, Kobayashi M (2015). Presynaptic cell type-dependent regulation of GABAergic synaptic transmission by nitric oxide in rat insular cortex. Neuroscience 284: 65-77.

Yamamoto T (1984). Taste responses of cortical neurons. Prog Neurobiol 23: 273-315.

Yasui Y, Breder CD, Saper CB, Cechetto DF (1991). Autonomic responses and efferent pathways from the insular cortex in the rat. J Comp Neurol 303: 355-374.

Yokota E, Koyanagi Y, Yamamoto K, Oi Y, Koshikawa N, Kobayashi M (2016). Opioid subtype- and cell-type-dependent regulation of inhibitory synaptic

transmission in the rat insular cortex. Neuroscience 339: 478-490.

Table and Figures

Table 1. Intrinsic electrophysiological properties of layer V interneurons

Interneuron subtype	Pyramidal neurons		Fast-spiking neurons	
	CAP	Sham	CAP	Sham
n[†]	74	65	43	35
N[†]	22	22	21	22
Vm[†] (mV)	-68.2 ± 0.7	-69.4 ± 0.7	-67.2 ± 0.8	-68.1 ± 0.7
Input resistance (MΩ)	134.7 ± 5.8	121.1 ± 5.3	125.1 ± 4.9	120.5 ± 4.2
Action potential				
Threshold (mV)	-42.5 ± 0.5	-42.3 ± 0.4	-40.9 ± 0.6	-40.5 ± 0.6
Amplitude (mV)	116.5 ± 1.0	114.9 ± 1.6	88.5 ± 1.5	88.7 ± 1.5
Rheobase (pA)	95.1 ± 4.8	105.3 ± 5.7	143.9 ± 9.9	163.6 ± 18.5
Half duration (ms)	2.6 ± 0.1	2.8 ± 0.2	1.1 ± 0.1	1.0 ± 0.0
Repetitive firing				
Max[††] (Hz)	26.4 ± 0.8	26.8 ± 0.7	93.2 ± 3.6	97.3 ± 9.2
Slope (Hz/pA)	0.025 ± 0.001	0.025 ± 0.001	0.083 ± 0.005	0.097 ± 0.013

[†]The number of cells (n) and animals (N); [††]Resting membrane potential; [†††]The number of maximum firing rate.

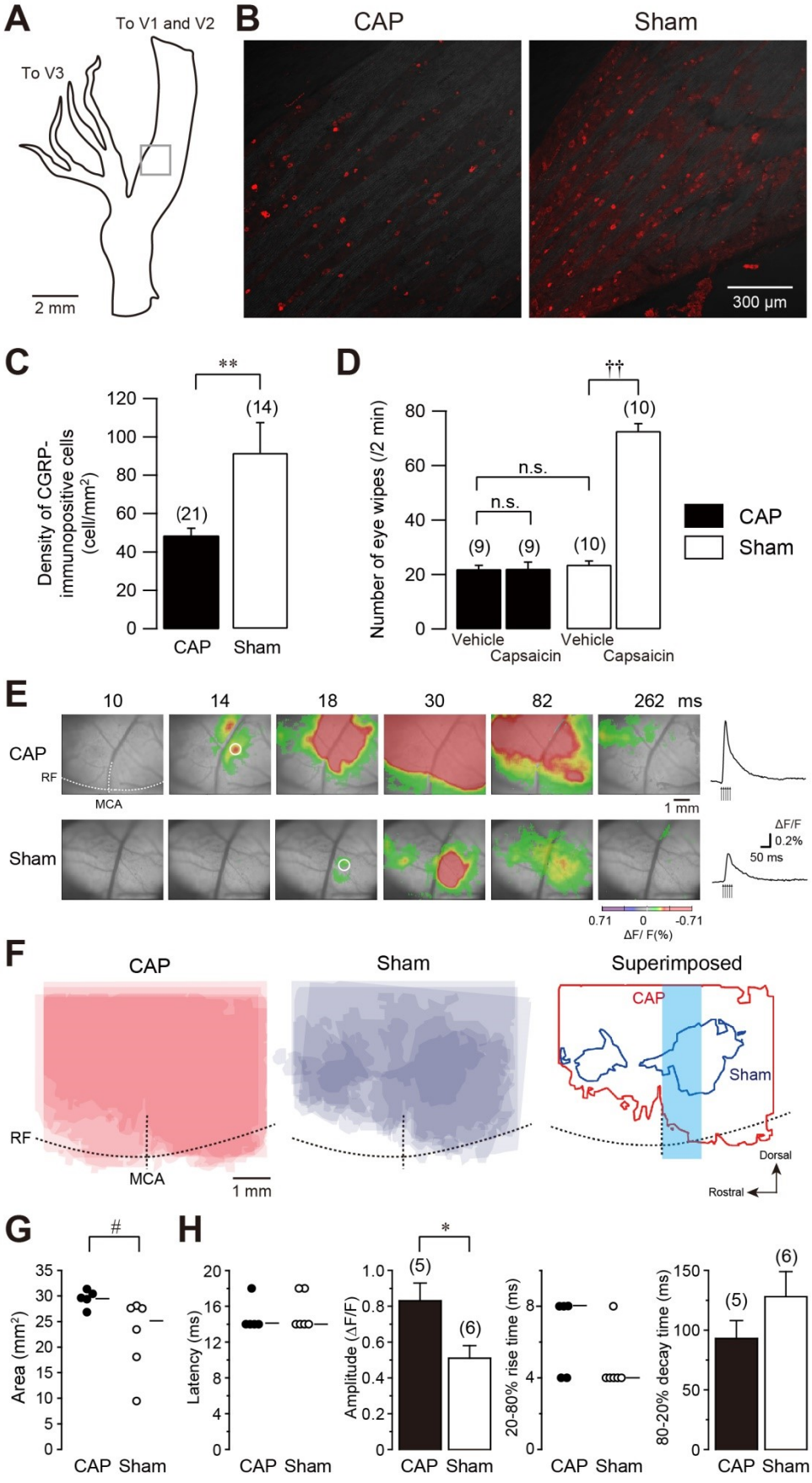
A
To V1 and V2
To V3
2 mm
B
CAP
Sham
300 μm
C
**
(14)
(21)
Density of CGRP-immunopositive cells (cell/mm²)
120
100
80
60
40
20
0
CAP
Sham
D
††
(10)
n.s.
n.s.
(9)
(9)
(10)
Number of eye wipes (/2 min)
80
60
40
20
0
Vehicle
Capsaicin
Vehicle
Capsaicin
CAP
Sham
E
10
14
18
30
82
262 ms
CAP
RF
MCA
1 mm
Sham
ΔF/F
0.2%
50 ms
0.71
0
-0.71
ΔF/ F(%)
F
CAP
Sham
Superimposed
RF
MCA
1 mm
CAP
Sham
Dorsal
Rostral
G
#
Area (mm²)
35
30
25
20
15
10
5
0
CAP
Sham
H
*
Latency (ms)
20
16
12
8
4
0
CAP
Sham
(5)
(6)
Amplitude (ΔF/F)
1.0
0.8
0.6
0.4
0.2
0
CAP
Sham
20-80% rise time (ms)
8
4
0
CAP
Sham
(5)
(6)
80-20% decay time (ms)
150
100
50
0
CAP
Sham

Fig. 1. Quantification of CGRP-immunopositive cells in the trigeminal ganglion, eye-wiping test, and optical imaging

A, the region of interest for the estimation of the density of CGRP-immunopositive cells in the trigeminal ganglion. *B*, examples of the distribution of CGRP-immunopositive cells in a capsaicin-treated (CAP) and vehicle-treated rat (Sham). *C*, the density of CGRP-immunopositive cells in CAP (N = 21) is less than that in Sham (N = 14). *D*, The number of eye-wiping for 2 min responding to vehicle and to 0.01% capsaicin to the eye. In contrast to more frequent eye-wiping to capsaicin than to vehicle in Sham (N = 10), CAP shows a comparable frequency of eye-wiping to capsaicin and vehicle (N = 9). *E*, Color-coded optical signals evoked by electrical stimulation to the maxillary 1st molar pulp in CAP and Sham. The time from the onset of electrical stimulation (arrows) is shown at the top of each panel. Temporal profiles of optical signals in the region of interests (white circles) are shown on the right panels. *F*, Superimposed maximum responses to stimulation of the maxillary 1st molar obtained from 5 CAP (left) and 6 Sham (middle). Superimposed outlines of the maximum responses, which overlapped in all CAP (red) and Sham (purple), are shown on the right. The blue-colored rectangle indicates the region from which the slices are prepared. *G*, comparison of the area of excitation between CAP and Sham. *H*, the latency, amplitude, 20-80% rise time, and 80-20% decay time of optical signal in the center of the initially excited region in CAP and Sham. The horizontal bars in (*G*) and (*H*) indicate the median. The number of animals is shown on the top of each bar.*: $P < 0.05$, **: $P < 0.01$, Student's *t*-test; ††: $P < 0.01$, n.s.: not significant, Student's *t*-test with Bonferroni correction; #: $P < 0.05$, Mann–Whitney *U* test.

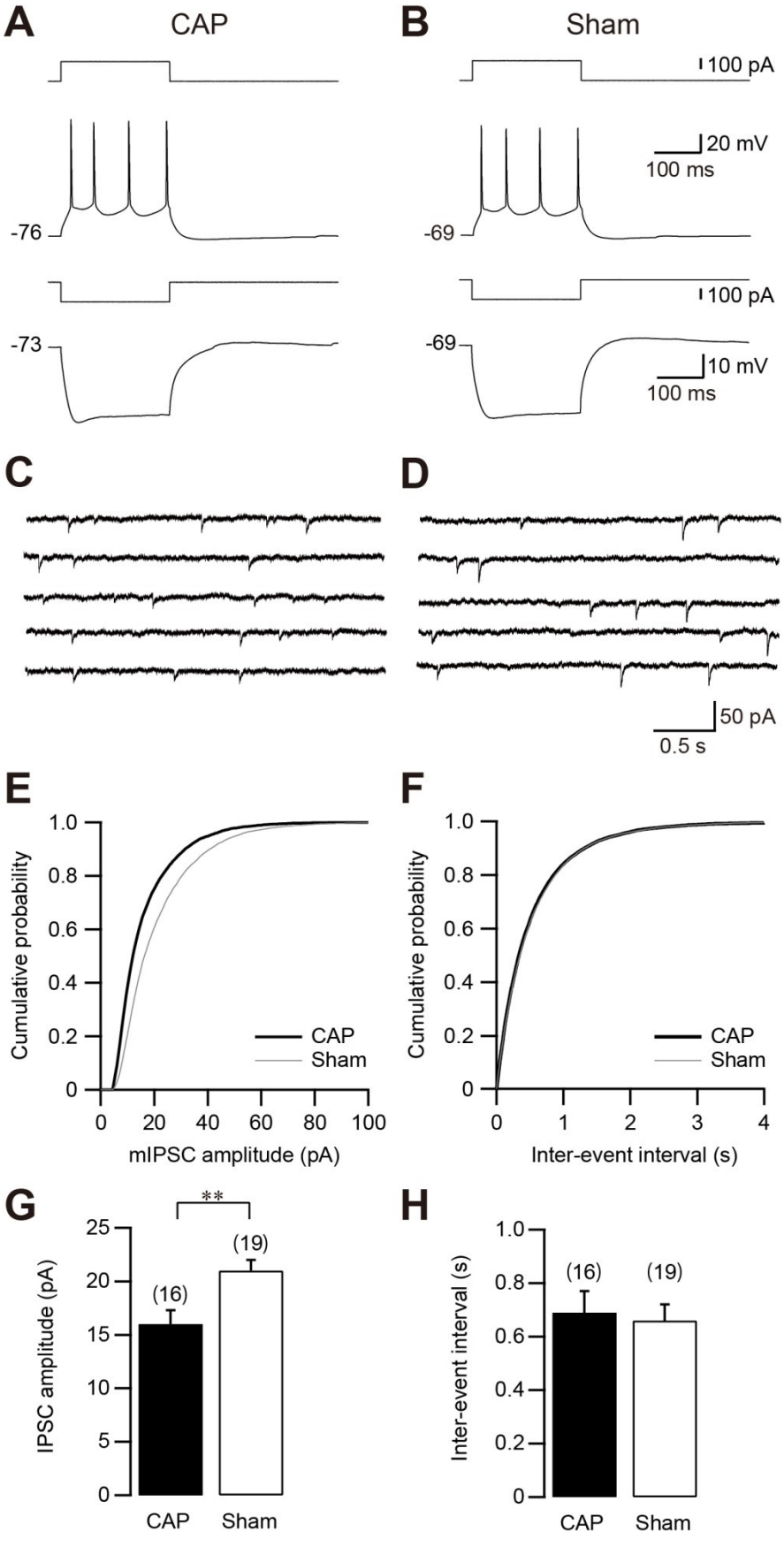
A
CAP
100 pA
20 mV
100 ms
-76
-73
B
Sham
100 pA
-69
-69
10 mV
100 ms
C
D
50 pA
0.5 s
E
Cumulative probability
1.0
0.8
0.6
0.4
0.2
0
0
20
40
60
80
100
mIPSC amplitude (pA)
CAP
Sham
F
Cumulative probability
1.0
0.8
0.6
0.4
0.2
0
0
1
2
3
4
Inter-event interval (s)
CAP
Sham
G
**
IPSC amplitude (pA)
25
20
15
10
5
0
(16)
(19)
CAP
Sham
H
Inter-event interval (s)
1.0
0.8
0.6
0.4
0.2
0
(16)
(19)
CAP
Sham

Fig. 2. Profiles of miniature IPSCs obtained from pyramidal neurons

A and B, representative voltage responses to depolarizing and hyperpolarizing current pulse injection to pyramidal neurons (Pyr) in CAP (*A*) and Sham (*B*). Almost comparable voltage responses are observed. The resting membrane potential is shown on the left of each trace. *C and D*, miniature IPSCs (mIPSCs) recorded under application of 1 μM TTX, 25 μM D-APV, and 20 μM DNQX. Traces in (*C*) and (*D*) were obtained from the same Pyr shown in (*A*) and (*B*), respectively. Holding potential was set at -70 mV. Calibrations in (*B*) and (*D*) are also applied to (*A*) and (*C*), respectively. *E and F*, The cumulative plots of the amplitude (*E*) and inter-event interval (*F*) obtained from the sum of 16 CAP (thick) and 19 Sham (thin). Note that the cumulative plot of CAP mIPSC amplitude showed the leftward shift in comparison to that of Sham. *G and H*, the mean amplitude (*G*) and inter-event interval (*H*) of CAP (n = 16) and Sham (n = 19). CAP showed the smaller amplitude of mIPSCs than Sham. **: $P < 0.01$, Student's *t*-test.

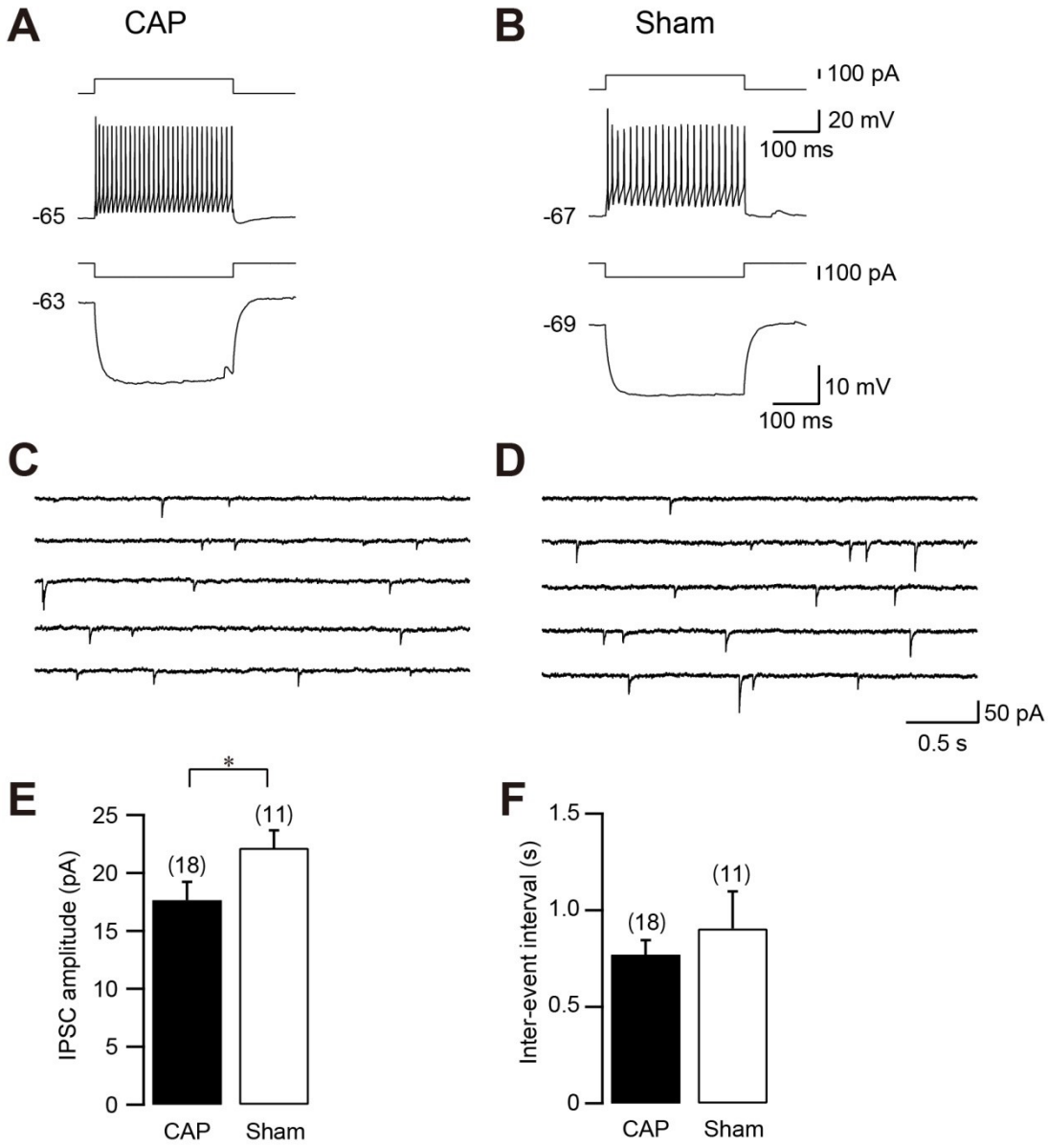

Fig. 3. Profiles of miniature IPSCs obtained from fast-spiking neurons

A and B, Example voltage responses to depolarizing and hyperpolarizing current pulse injection to fast-spiking neurons (FS) in CAP (*A*) and Sham (*B*). The resting membrane potential is shown on the left of each trace. *C and D*, representative traces of miniature IPSCs (mIPSCs) in the presence of 1 μM TTX, 25 μM D-APV, and 20 μM DNQX. Traces in (*C*) and (*D*) were obtained from the same FS shown in (*A*) and (*B*), respectively. mIPSCs were recorded with membrane potential holding at -70 mV. Calibrations in (*B*) and (*D*) are also applied to (*A*) and (*C*), respectively. *E and F*, the mean amplitude (*E*) and inter-event interval (*F*) of CAP (n = 18) and Sham (n = 11). CAP showed the smaller amplitude of mIPSCs than Sham in FS. *: $P < 0.05$, Student's *t*-test.

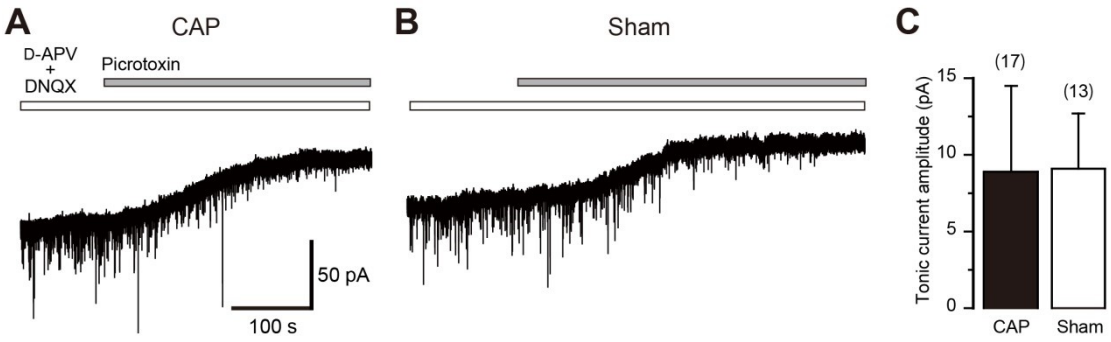

Fig. 4. GABAergic tonic currents recorded from pyramidal neurons

A and B, Spontaneous IPSC recording from Pyr in CAP (*A*) and Sham (*B*) under application of 25 μM D-APV and 20 μM DNQX. Additional application of 100 μM picrotoxin induced outward shift of the holding current. Note the disappearance of spontaneous IPSCs after application of picrotoxin. *C,* Little difference in GABAergic tonic currents between CAP (n = 13) and Sham (n = 17).

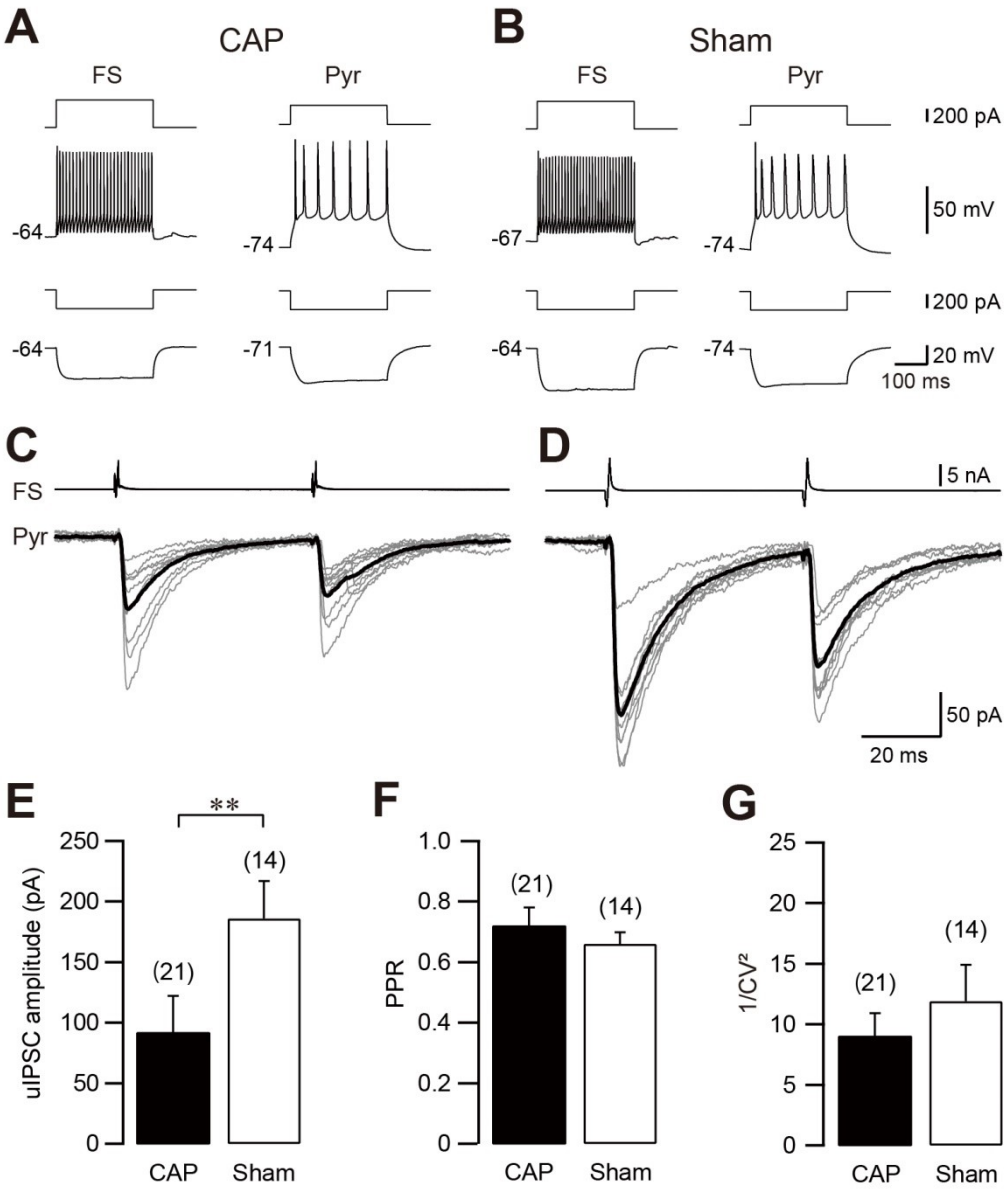

Fig. 5. Profiles of unitary IPSCs in FS→Pyr connections.

A and B, typical spike firing examples of fast-spiking (FS) and Pyr of CAP (*A*) and Sham (*B*), showing comparable voltage responses between CAP and Sham. FS exhibited large and fast afterhyperpolarization and high-frequency spike firing without adaptation, while Pyr showed regular spike firing with adaptation. *C and D*, unitary IPSCs (uIPSCs) recording by paired whole-cell patch-clamp recordings from FS and Pyr in CAP (*C*) and Sham (*D*). Action potentials were elicited in presynaptic FS (middle) by application of short depolarizing voltage pulses (80 mV, 2 ms, top), and uIPSCs were recorded from postsynaptic Pyr. Fifteen consecutive traces are shown in grey lines, and the averaged traces were shown in thick black lines. Calibrations in (*B*) and (*D*) are also applied to (*A*) and (*C*), respectively. *E, F and G*, the peak amplitude (*E*), paired-pulse ratio (PPR; *F*), and the inverse of squared coefficient of variation ($1/CV^2$, *G)* of uIPSCs in CAP and Sham. Note that CAP shows smaller amplitude of uIPSCs than Sham without changing PPR and $1/CV^2$. **: $P < 0.01$, Student's *t*-test.

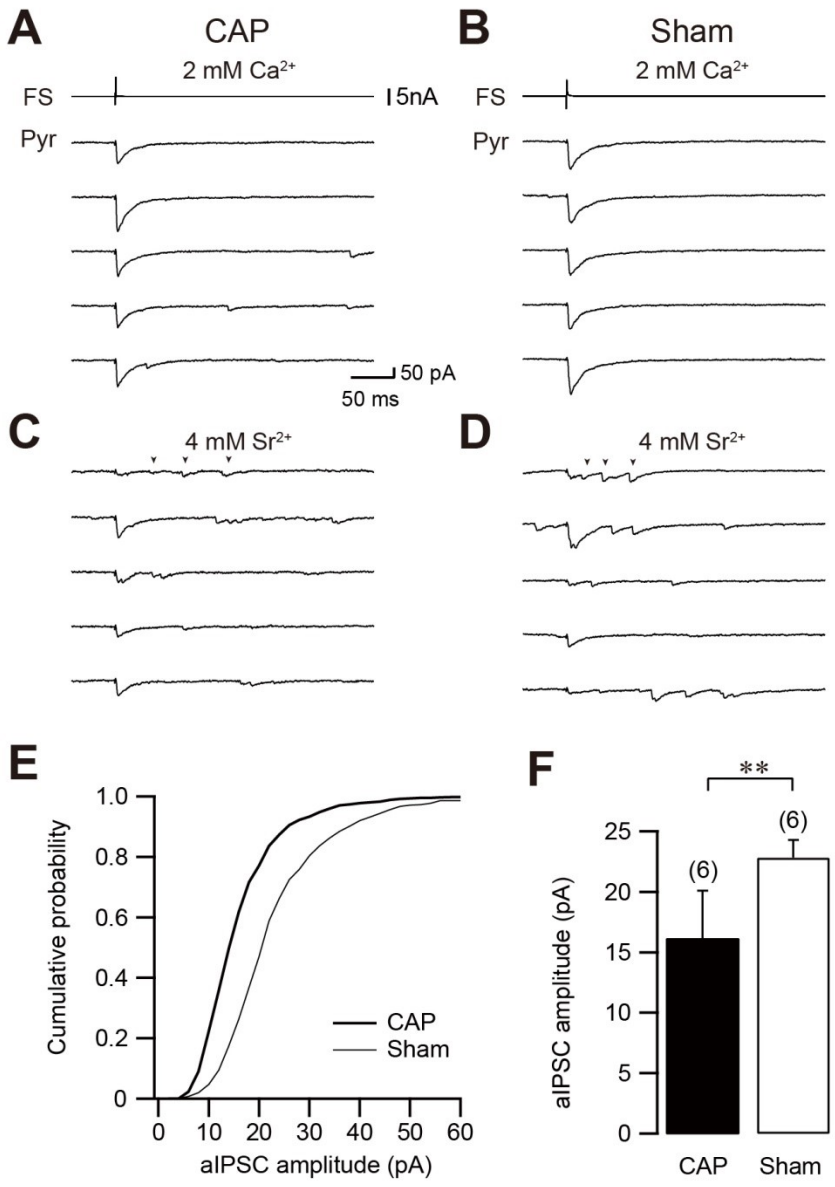

Fig. 6. Profiles of asynchronous IPSCs in FS→Pyr connections

A and B, uIPSCs obtained from FS→Pyr connections in CAP (*A*) and Sham (*B*). Five consecutive traces are shown. *C and D*, by replacing 2 mM Ca^{2+} to Sr^{2+}, the amplitude of uIPSCs shown in (*A*) and (*B*) became smaller both in CAP (*C*) and Sham (*D*), respectively. These smaller uIPSCs frequently accompanied IPSCs that occurred irregularly, asynchronous IPSCs (aIPSCs). Calibration in (*A*) is also applied to (*B-D*). *E*, the cumulative plot of the amplitude of aIPSCs of CAP (thick) was shifted toward left compared to that of Sham (thin), suggesting that aIPSCs obtained from CAP shows smaller amplitude. *F*, the mean amplitude of aIPSCs in CAP was smaller than that in Sham. **: $P < 0.01$, Student's *t*-test.

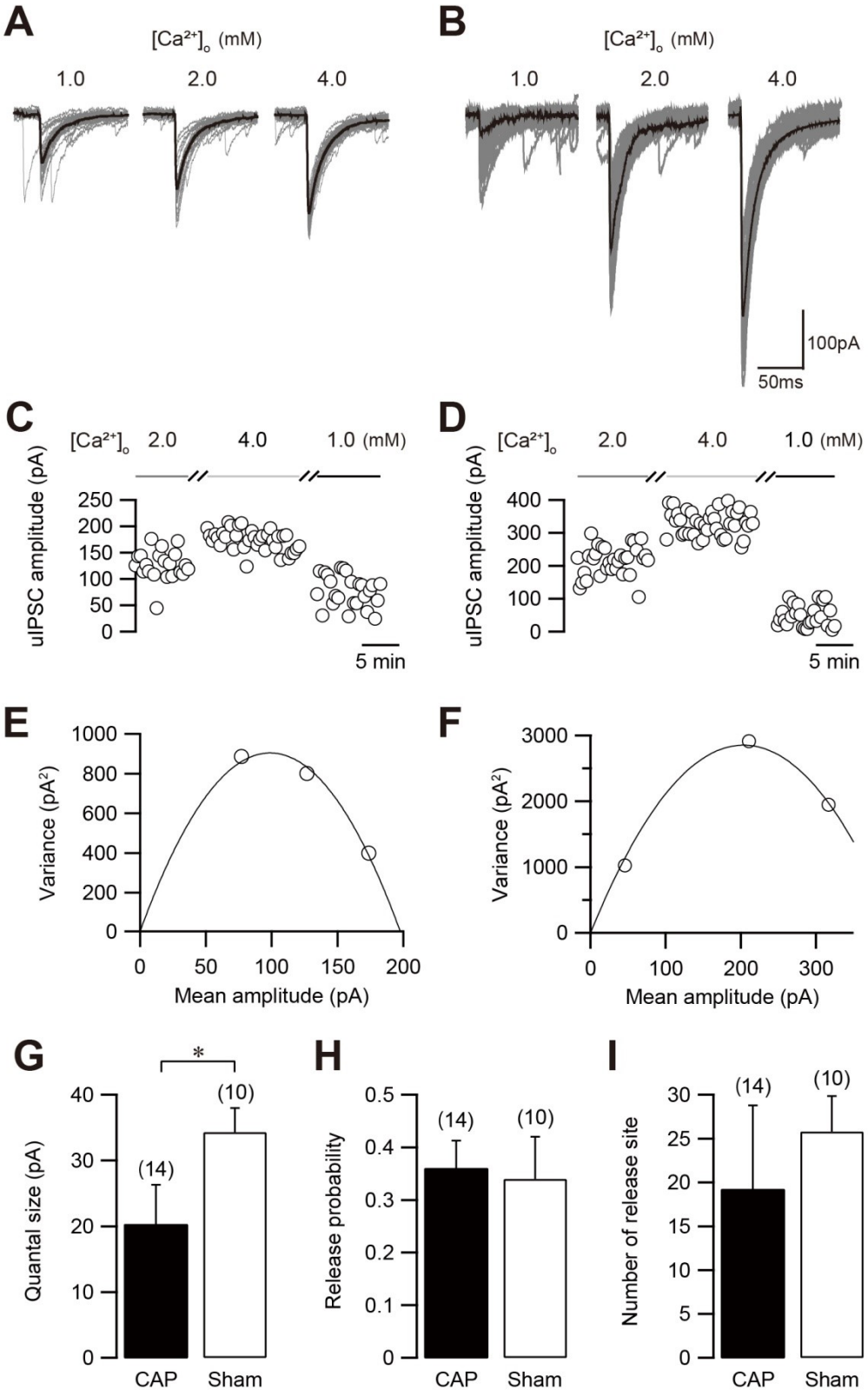
A
[Ca2+]o (mM)
1.0
2.0
4.0
B
[Ca2+]o (mM)
1.0
2.0
4.0
100pA
50ms
C
[Ca2+]o 2.0 4.0 1.0 (mM)
uIPSC amplitude (pA)
250
200
150
100
50
0
5 min
D
[Ca2+]o 2.0 4.0 1.0 (mM)
uIPSC amplitude (pA)
400
300
200
100
0
5 min
E
Variance (pA2)
1000
800
600
400
200
0
0 50 100 150 200
Mean amplitude (pA)
F
Variance (pA2)
3000
2000
1000
0
0 100 200 300
Mean amplitude (pA)
G
*
Quantal size (pA)
40
30
20
10
0
(14)
(10)
CAP
Sham
H
Release probability
0.5
0.4
0.3
0.2
0.1
0
(14)
(10)
CAP
Sham
I
Number of release site
30
25
20
15
10
5
0
(14)
(10)
CAP
Sham

Fig. 7. Variance-mean analysis of uIPSCs in FS→Pyr connection

A and B, V-M analysis of representative FS→Pyr connections in CAP (*A*) and Sham (*B*). $[Ca^{2+}]_o$ was changed from 1.0 to 4.0 mM. Calibrations in (*B*) are also applied to (*A*). *C and D*, the uIPSC amplitude in response to different $[Ca^{2+}]_o$ in consecutive trials shown in (*A*) and (*B*). *E and F*, plotted data showing relationship between the mean IPSC amplitude and their variance were fitted by a quadratic function. Both are from the same neurons shown in (*A*) and (*B*), respectively. *G, H, and I*, Summary of estimated quantal size (*G*), release probability (*H*), and number of release site (*I*). Note that reduction of quantal size (*G*) is observed in CAP, however release probability (*H*) and the number of release site (*I*) were not different between CAP and Sham.